Self-Assembled Phases of Block Copolymer Blend Thin Films

Kevin G. Yager, Erica Lai, and Charles T. Black*

Center for Functional Nanomaterials, Brookhaven National Laboratory, Upton, New York 11973, United States

ABSTRACT The patterns formed by self-assembled thin films of blended cylindrical and lamellar polystyrene-*b*-poly(methyl methacrylate) block copolymers can be either a spatially uniform, single type of nanostructure or separate, coexisting regions of cylinders and lamellae, depending on fractional composition and molecular weight ratio of the blend constituents. In blends of block copolymers with different molecular weights, the morphology of the smaller molecular weight component more strongly dictates the resulting pattern. Although molecular scale chain mixing distorts microdomain characteristic length scales from those of the pure components, even coexisting morphologies exhibit the same domain spacing. We quantitatively account for the phase behavior of thin-film blends of cylinders and lamellae using a physical, thermodynamic model balancing the energy of chain distortions with the entropy of mixing.

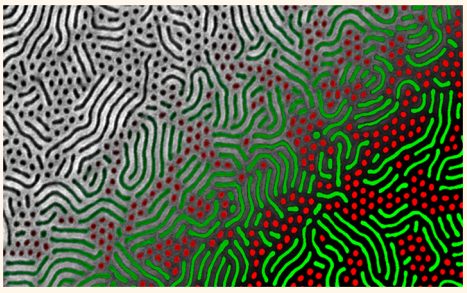

KEYWORDS: block copolymers · thin films · block copolymer blends · self-assembly · phase diagram

The ability of block copolymers to autonomously assemble into regular patterns with uniform, nanometer-scale features, and their straightforward integration with techniques of thin-film processing and device fabrication, have rendered them highly appealing as patterning materials for information technology,[1] and other technological applications in energy,[2] membranes,[3] and fluidics.[4] While the feature sizes of patterns formed by block copolymer thin films may be tuned through either copolymer molecular weight[5] or by blending with homopolymers,[6−9] the pattern morphology generally exhibits a single repeating structure (*e.g.*, sphere, cylinder, lamellae) within the thin film layer.

In this work, we quantitatively study the phase morphology of thin films composed of blended cylinder- and lamellar-forming polystyrene-*b*-poly(methyl methacrylate) (PS-*b*-PMMA) block copolymers in order to understand the conditions and requirements for generating patterns containing both morphologies simultaneously. Here, we focus on thin films with the nanoscale morphology extending uniformly through the entire film thickness, due to their relevance for patterning applications. Previous experimental investigations[10−15] and calculations[16,17] have shown that in the bulk, blends of block copolymers can result in either single-phase patterns or two coexisting phases.

Controlling the self-assembled morphology through blending facilitates application of block copolymers as patterning materials. A simple example is adjusting the pattern feature sizes and density through mixing block copolymers with homopolymers,[7,9,18,19] such that a small library of materials is sufficient for producing a broader array of sizes. In addition, the templating patterns used to guide block copolymer assembly in directed assembly applications[20−22] can, in principle, similarly guide the spatial makeup of multiple pattern morphologies in a blended copolymer film. Such a strategy has been used for local control of the domain orientation of a single-component block copolymer films in order to create patterns with two morphologies.[8,23−25]

RESULTS/DISCUSSION

First, we consider the patterns formed by self-assembled thin films made from lamellar PS-*b*-PMMA (with molecular weight M_w(lam) = 74 kg/mol) blended with increasing amounts of a similar M_w PS-*b*-PMMA cylindrical material [M_w(cyl) = 67 kg/mol]. Some mixing ratios give rise to patterns containing coexisting lamellar lines/spaces and hexagonally arranged cylinder dot arrays (Figure 1). The M_w ratio of the components

* Address correspondence to ctblack@bnl.gov.

Received for review July 22, 2014 and accepted September 29, 2014.

Published online October 06, 2014
10.1021/nn504977r

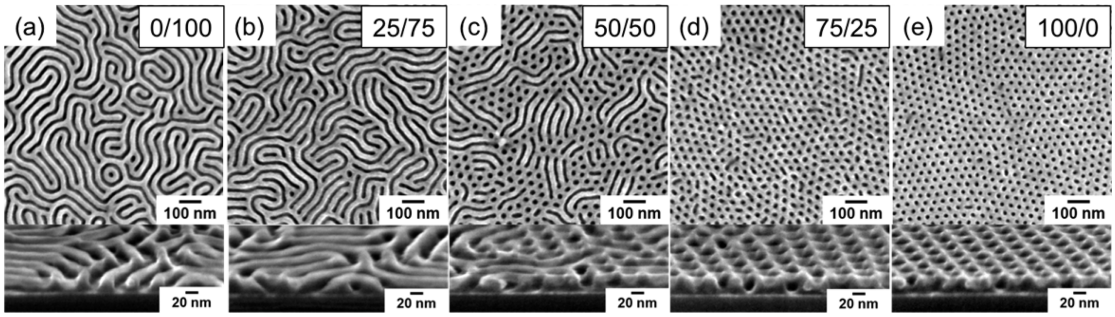

Figure 1. Top-down and 70° tilt SEM images of thin film blends of 67 kg/mol cylindrical phase and 74 kg/mol lamellar phase PS-*b*-PMMA. The M_w ratio of the blend components is M_w(cyl)/M_w(lam) = 0.9. The weight ratios (m_c/m_l) of cylinder/lamellae blends are (a) 0/100 (pure lamellar), (b) 25/75, (c) 50/50, (d) 75/25, and (e) 100/0 (pure cylindrical). We have cross-linked the PS block and chemically removed the PMMA for improved SEM contrast using techniques described in the text.

in this blend is M_w(cyl)/M_w(lam) = 0.9 ≈ N(cyl)/N(lam), where N denotes the numbers of monomers in the chains, with the last approximate equality holding because of the similar formula weights of PS and PMMA (~100 g/mol). From Fourier transforms of the scanning electron microscope (SEM) images, we measure characteristic domain spacings of the pure lamellar and cylindrical phases of ℓ_0(lam) = 41 nm and ℓ_0(cyl) = 35 nm, where ℓ_0(lam) is the lamellar repeat period and ℓ_0(cyl) is the spacing between adjacent cylinder rows (Supporting Information). In these experiments, we treat the surface with a PS-*r*-PMMA random copolymer brush layer prior to forming the block copolymer blend thin film, in order to promote perpendicular orientation of the block copolymer domains,[26,27] and thermally anneal at sufficiently high temperature (200 °C) to equalize the surface tensions of PS and PMMA. We use both top-down and cross-sectional scanning electron microscopy (SEM) to confirm the perpendicular domain orientation for all thin films studied here, including single-component cylindrical and lamellar phases and all blend compositions. We spin-cast blended block copolymers from solution, targeting formation of films with domains running perpendicularly through the entire 26 ± 2 nm thickness, measured from SEM images (Figure 1). We facilitate self-assembly by annealing in vacuum (<1 Torr) for at least 16 h, verifying that this amount of time is sufficiently long to establish patterns with unchanging fractional areal coverage of lamellae and cylinders (Supporting Information). Single component films of both lamellar (Figure 1a) and cylindrical (Figure 1e) materials form uniform patterns consistent with the two pure block copolymer phases, while patterns formed by blends with increasing cylinder content contain increasing fractional areas of dots (cylinder morphology) (Figures 1b–d), qualitatively similar to previous bulk studies of blends of styrene-*b*-isoprene blends.[13,15] The m_c/m_l = 50/50 weight cylinder/lamellae blend (where m_c and m_l are the masses of the cylindrical and lamellar copolymers in the blend) generates a pattern with approximately equal parts cylinder and lamellae coverage (Figure 1c). Cross-sectional SEM images of blend films show a uniform 2D morphology consistent with a mixture of perpendicularly oriented cylindrical and lamellar domains (Figure 1).

Changing the M_w ratio of the blend components alters the nature by which the self-assembled pattern evolves from being purely line/space (lamellar) to a hexagonal dot array (cylindrical) with increasing amount of the cylinder-forming component. For example, blending the same M_w(lam) = 74 kg/mol lamellar material instead with a *lower* molecular weight cylindrical PS-*b*-PMMA [M_w(cyl) = 48 kg/mol] (M_w(cyl)/M_w(lam) = 0.65) results in patterns that transition more abruptly to pure dot arrays with increasing cylinder content (Figure 2a–e, film thickness = 26 ± 2 nm); that is, a surprisingly small mass fraction of the cylindrical material (<50%) is sufficient to yield a nearly pure cylindrical morphology. In particular, both the m_c/m_l = 50/50 (Figure 2c) and 75/25 (Figure 2d) cylinder/lamellae mixtures form patterns with a largely single morphology resembling that of a pure cylindrical material (Figure 2e). In contrast, patterns formed by blend mixtures of the M_w(lam) = 74 kg/mol lamellar PS-*b*-PMMA with a *higher* molecular weight cylindrical material [M_w(cyl) = 99 kg/mol] (M_w(cyl)/M_w(lam) = 1.34) (Figure 2f–j, film thickness = 25 ± 2 nm) retain a significant fractional coverage of the line/space (lamellar) pattern at a m_c/m_l = 50/50 ratio (Figure 2h). Thus, contrary to expectations, the areal fractions of coexisting morphologies are not simply dictated by the mass, or volume, fractions of the mixed copolymer species.

In the two examples of blends with components having dissimilar molecular weights, it is the phase of the *lower* molecular weight component that more heavily influences the overall pattern, generally consistent with the pattern morphology being dictated by the blend component contributing the *larger number of chains* to the mixture. For example, a m_c/m_l = 50/50 weight mixture of equal M_w cylinders and lamellae contains the same number of cylindrical and lamellar molecules, and yields a pattern with similar fractional

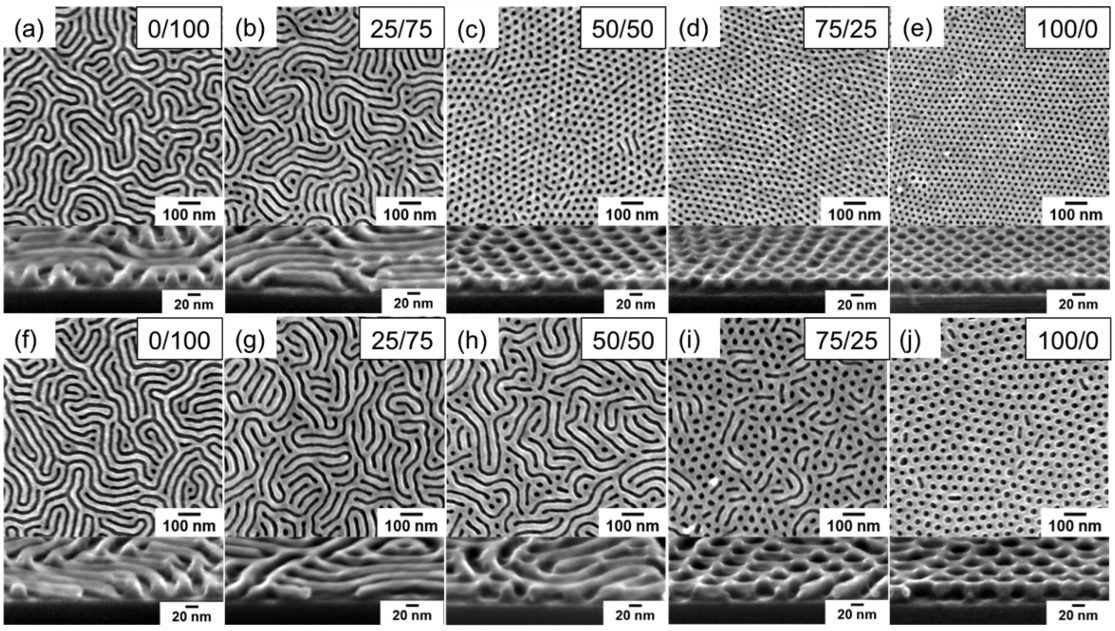

Figure 2. (a–e) Top-down and 70° tilt SEM images of thin film blends of 48 kg/mol cylindrical phase and 74 kg/mol lamellar phase PS-*b*-PMMA. The M_w ratio of the blend components is M_w(cyl)/M_w(lam) = 0.65. The weight ratios (m_c/m_l) of cylinder/lamellae blends are (a) 0/100 (pure lamellar), (b) 25/75, (c) 50/50, (d) 75/25, and (e) 100/0 (pure cylindrical). (f–j) Top-down SEM images of thin film blends of 99 kg/mol cylindrical phase and 74 kg/mol lamellar phase PS-*b*-PMMA. The M_w ratio of the blend components is M_w(cyl)/M_w(lam) = 1.34. The weight ratios (m_c/m_l) of cylinder/lamellae blends are (f) 0/100 (pure lamellar), (g) 25/75, (h) 50/50, (i) 75/25, and (j) 100/0 (pure cylindrical). We have cross-linked the PS block and chemically removed the PMMA for improved SEM contrast using techniques described in the text.

coverage of each (Figure 1c). However, a 50/50 weight mixture of higher M_w lamellae mixed with smaller cylinders contains M_w(lam)/M_w(cyl) times more cylinder molecules compared to lamellar, and produces a largely cylindrical pattern (Figure 2c). Similarly, an equal weight mixture of higher M_w cylinder molecules and smaller lamellae yields a predominantly lamellar pattern (Figure 2h). The fractional number of cylindrical (f_{cyl}) and lamellar (f_{lam}) molecules in any blend ratio is

$$f_{cyl} = \frac{1}{1 + \dfrac{M_w(\text{cyl})/M_w(\text{lam})}{m_c/m_l}} \quad (1a)$$

$$f_{cyl} + f_{lam} = 1 \quad (1b)$$

Through image analysis of the SEM measurements, we quantify the progression of a purely lamellar pattern to purely cylindrical one with increasing blend fractions of cylinder forming material, for each of the three blend component molecular weight ratios studied (Supporting Information). For blends of *similar* cylinder and lamellae molecular weights [M_w(cyl)/M_w(lam) = 0.9], the fraction of the pattern area covered by cylinders loosely tracks cylinder mass fraction in the blend, increasing smoothly to 15% at m_c/m_l = 25/75 blend composition, to 63% at 50/50, and 92% at 75/25 (Figure 3a, black circles). Patterns formed from blends of cylinders and lamellae with *dissimilar* total molecular weights transition more abruptly. For example, while a pattern formed from a m_c/m_l = 25/75 mixture with M_w(cyl)/M_w(lam) = 0.65 contains 11% cylinder area coverage, the fractional coverage increases to >85% at 50/50 composition (Figure 3a, blue circles). Similarly, a m_c/m_l = 75/25 mixture with M_w(cyl)/M_w(lam) = 1.34 forms patterns with >60% cylinders, but reduces to <10% in a 50/50 blend (Figure 3a, red circles).

The differences between the pattern's fractional coverage of cylindrical and lamellar domains and the fractional composition of blend components imply that the two materials are mixed at a molecular level. However, two morphologies coexisting in a single pattern suggests that the energy minimum sometimes involves only partial mixing of the chains, with the two distinct phases each having a different ratio of the two blended chains. A consequence of the molecular mixing is distortion in the characteristic domain spacings (ℓ) of the lamellar [ℓ(lam)] and cylindrical [ℓ(cyl)] microdomains from those of the pure components (denoted as ℓ_0). We quantify the distortion by measuring changes in average domain spacing within the cylindrical and lamellar pattern regions (Figure 3b). Both ℓ(lam) and ℓ(cyl) vary continuously from their single component values as the two materials are blended together. Furthermore, the patterns formed by all blend mixtures show a single characteristic domain spacing, given approximately by ℓ(lam) = ℓ(cyl) = $\ell \sim [f_{cyl} \times \ell_0(\text{cyl}) + f_{lam} \times \ell_0(\text{lam})]$, irrespective of whether the film has a single morphology (lamellae, or cylinders) or separate regions of cylinders and lamellae (Figure 3b). The well-matched domain spacings in

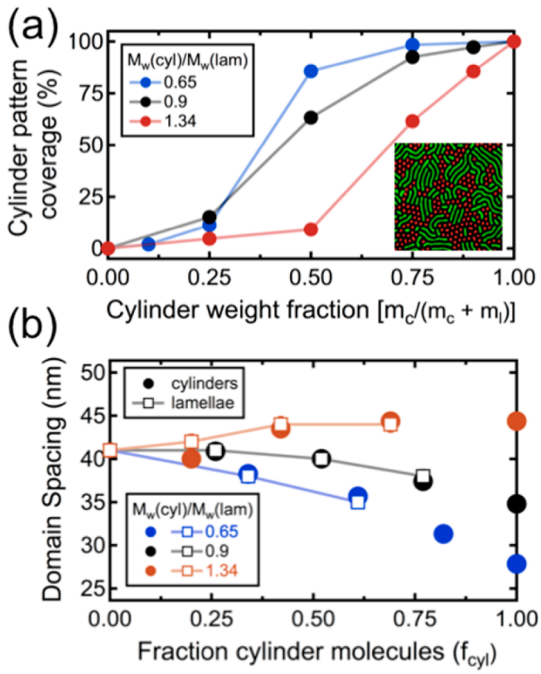

Figure 3. (a) Percentage areal coverage of the cylindrical phase pattern *versus* weight percentage of cylindrical phase block copolymer in the cylinder/lamellae block copolymer blend. The average total molecular weight ratio of cylindrical to lamellar is (blue) 0.65, (black) 0.9, and (red) 1.34. Inset: Colorized SEM image showing cylinders (red) and lamellae (green) coverage. (b) Measured average domain spacing for cylinders (circles) and lamellae (squares) *versus* the fraction of cylindrical phase block copolymer molecules in the cylinder/lamellae block copolymer blends. Error bars denote a ±2% uncertainty in the average domain spacing, from the standard deviation of fundamental peak positions in the FFT of the SEM images. The average total molecular weight ratio of cylindrical to lamellar is (blue) 0.65, (black) 0.9, and (red) 1.34.

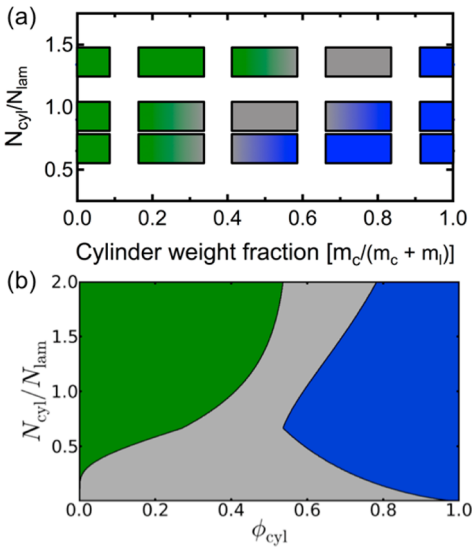

Figure 4. (a) Phase diagram showing the observed pattern morphology (green = lamellar, gray = mixed cylinders and lamellae, blue = cylindrical) *versus* the cylinder weight fraction in the blend. Plotted for three different blend component molecular weight ratios. Squares with graded shadings represent patterns that straddle the condition defining a single phase (patterns with ≥90% of one morphology). (b) Phase diagram calculated from free energies of chain distortions accompanying blending different block copolymers (see Supporting Information). The presented example mixes cylinder-forming and lamellae-forming materials, for different molecular-weight ratios (N_{cyl}/N_{lam}), and volumetric mixing fraction (ϕ_{cyl}). Regions show either a single lamellar (green) or cylinder (blue) morphology, or both phases simultaneously (gray).

separate cylindrical and lamellar regions within a single film provide a lower energy penalty at the boundaries between regions, because the two distinct morphologies can align with one another. We can observe this registry between adjacent morphologies in the SEM data. For example, the PMMA domains of the lamellar phase align with the rows of PMMA cores in adjacent cylinder phases (see, for example, Figure 1c), as required to maintain energetically favorable chain packing at the domain interfaces. Thus, a uniform ⁄ across the different distinct phases necessarily arises from an energy-minimum for a particular intermixing of chains from the energy balance between chain distortions and entropy.

We construct phase diagrams for blended cylinder/lamellar block copolymer thin films by plotting the M_w ratio of the blend components (N_{cyl}/N_{lam}) *versus* the cylinder weight percentage [m_c/(m_c + m_l)], with regions color coded according to whether the resulting pattern is a single phase (lamellar (green color), or cylindrical (blue color)), or a two-component morphology (gray color) (Figure 4a). Blend compositions coded with mixtures of two colors are those that straddle our condition defining a single phase (patterns containing ≥90% of one morphology), and are assumed to be at the phase boundary. The phase diagram makes clear that the molecular weight ratio of the blended materials strongly influences the final morphological composition of the film with, for example, higher weight fractions of cylinder-material required to form a cylindrical morphology when mixing higher M_w cylinders with smaller lamellae. The blend phase diagram provides a method for generating prescribed pattern morphologies from a small library of block copolymers. For example, it is possible to realize a particular phase having a prescribed domain spacing by blending competing morphologies with a carefully selected molecular weight ratio. Moreover, the broad region of coexisting phases provides exciting opportunities for prescribing patterns with exact areal fractions of coexisting morphologies and control over the domain spacing. Established methods in directed self-assembly could conceivably be used to localize such coexisting morphologies.

Compared to mixing of homopolymers, in blends of block copolymers the molecular architecture imposes an additional constraint on chain mixing. While enthalpy effects continue to drive the blend system toward microphase separation, copolymer chains of different M_w and/or block weight ratio must incur an

energy penalty upon mixing due to their competing equilibrium morphologies. For example, in order to uniformly distribute a small M_w chain within a larger morphology, either the small chain must stretch, and/or the larger chains must compress to compensate for the inability of the small chain to uniformly access the larger morphology. In either case, the chain distortions incur an energy penalty, which must be considered in assessing the final blend morphology. This chain distortion arises from the requirements of microphase separation that the point along each copolymer chain where chemical identity changes is necessarily pinned at the morphological interfaces.

To illuminate the physical origins of our experimental results, we consider a highly simplified model comparing the relative energies of two idealized cases: shorter chains (lower N) stretching to mix into a larger morphology, and longer chains (larger N) compressing to fit within a smaller morphology. For a Gaussian chain of N repeat units (each of length a), the radius of gyration is $R_G = a \times (N/6)^{1/2}$. The free energy required to stretch ($F_{stretch}$) or compress ($F_{compress}$) the chain to a distance R is[28,29]

$$\beta F_{stretch} = \frac{1}{4}\left(\frac{R}{R_G}\right)^2 \quad (2)$$

$$\beta F_{compress} = \pi^2\left(\frac{R_G}{R}\right)^2 \quad (3)$$

where $\beta \equiv 1/(k_BT)$ with k_B the Boltzmann constant and T the temperature. Including more realistic conditions such as self-avoidance, solvent effects, and strong confinement will modify the prefactors and exponents in eqs 2 and 3 without changing the essential physics.[29−33] The case of chain compression is closely related to the concept of a "reflected random walk" for polymer chains near interfaces.[34−37] Thus, a long block copolymer chain confined within a smaller morphology is effectively meandering through a confinement volume, with a random-walk configuration reflecting off the morphology interfaces. Crucially, these free energies are *per chain*, which emphasizes the energy penalty for the blend species present in larger *number* fraction (rather than weight fraction). Thus, when computing the total free energy of mixing of copolymer chains of different N (Supporting Information), we find that at 50/50 weight (or volume) fraction, the minimum free energy configuration compresses larger chains into the smaller morphology, because this arrangement requires distortion of a smaller *number* of chains. Heuristically, the *lower-M_w* copolymer chains more heavily dictate the blend morphology, consistent with our experimental results.

For blends of sufficiently different copolymer chains (*i.e.*, disparate N), the two components may not mix and will instead phase separate. Although the entropy of mixing always drives the system toward chain mixing, in some cases this gain may not exceed the cumulative energy penalty due to chain distortions. We elaborated our simple model to next consider chain distortions from mixing two block copolymer chains of different molecular weights (N_1 and N_2), and volume fractions (f_1 and f_2). The model balances distortion energies arising within *both* of the chemically distinct domains of the two morphologies, against the entropy of mixing (see Supporting Information for complete derivation). We thus explicitly consider: (1) block copolymer 1 mixing into the morphology of block copolymer 2; (2) the inverse mixing; (3) the blend components do not mix and two distinct morphologies are observed. For simplicity, we omit consideration of other possible scenarios, including the partial mixing of block copolymer chains into chemically incompatible domains, or the appearance of new morphologies. The general form of the energy balance in our model is

$$\beta\frac{F_{total}}{N_{total}} = \beta\frac{F_A}{N_{A,tot}}\phi_A + \beta\frac{F_B}{N_{B,tot}}\phi_B + \beta\frac{F_{mix}}{N_{total}} \quad (4)$$

$$\beta\frac{F_{mix}}{N_{total}} = \frac{\phi_1}{N_1}\ln\phi_{A1} + \frac{\phi_2}{N_2}\ln\phi_{A2} + \frac{\phi_1}{N_1}\ln\phi_{B1} + \frac{\phi_2}{N_2}\ln\phi_{B2} \quad (5)$$

where 1 and 2 denote the two different copolymers in the blend, $\phi_{1,2}$ are their volume fractions, and A and B denote the two chemically distinct parts of each copolymer chain. The free energy contributions, F_A and F_B, include chain distortion effects (eqs 2 and 3), whose exact form depends on the relative chain lengths (*i.e.*, M_w and block ratios). We calculate these energies relative to the case where copolymer chains do not intermix (*i.e.*, $\beta F_{nomix}/N_{total} = 0$), and have omitted enthalpy-of-mixing contributions because they are identical in all cases. The resulting computed phase diagram for blends of cylinder-forming and lamellae-forming block copolymers with different M_w ratios (Figure 4b) displays similar behavior to experiment (Figure 4a), with regions of predicted lamellar (green) and cylindrical (blue) morphologies asymmetric about $\phi = 0.5$ and the morphology of the lower-M_w species over-represented (*e.g.*, a predominance of lamellae for $N_{cyl}/N_{lam} > 1$). The central region of the diagram (gray) denotes the region where our model predicts that mixing is energetically unfavorable, and we experimentally observe two coexisting morphologies.

Although our simplified model neglects several important considerations required for a full quantitative simulation of the blended block copolymer system, it nevertheless provides an instructive guide for understanding the phase behavior, explaining the coexistence of morphologies as well as the relative areal fractions of observed phases. In particular, the overall energy balance suggested by our model is evidently borne out by the experimental data: there is a central

region where the energetic cost of fully mixing is too great, and the system instead partially segregates the chains, giving rise to two distinct morphologies. On either side, we observe a single morphology that arises due to complete mixing of the copolymer blend components. Our model ignores the effect that block copolymer chain mixing changes copolymer volume fractions within the two phases, and can thereby alter the morphology, although the experimental data clearly indicate that this is taking place: the domains spacings of the observed blended morphologies are distorted due to the chains mixed into them. In fact, even patterns exhibiting two distinct morphologies (which our model naively terms "no mixing") exhibit distortions resulting from substantial mixing of chains. Our model also assumes monodisperse blend components; however, chain polydispersity has previously been observed to play a role.[38] We have omitted contributions from interfacial energies and aspects of block copolymer commensurability, because our experimental system consists of perpendicular morphologies that span the entire film thickness. The model neglects the overall interfacial curvature of copolymer domains, which is a crucial piece for predicting the possible appearance of new morphologies resulting from blending.

CONCLUSIONS

We have explored the landscape of morphologies arising from thin film blends of block copolymers with different intrinsic morphologies and disparate molecular weights. While the chemical compatibility of the corresponding blocks facilitates mixing, the mixing can be incomplete due to the energy penalty of distorting copolymer chains to fit within foreign morphologies. This results in a broad range of blend mixtures where multiple morphologies coexist, with matched domain spacings driven by molecular chain intermixing. In regimes with complete mixing, the ultimate morphology is preferentially dictated by the lower molecular weight blend component. Our results suggest that the observed behaviors will occur generally in thin films of blended copolymers, including those with high degrees of immiscibility and/or smaller characteristic length scales. Thus, this detailed understanding and control of morphology may facilitate new and more complex applications of self-assembling block copolymer thin films as patterning materials.

EXPERIMENTAL SECTION

Block Copolymer Thin Film Preparation. For these experiments, we used 500 μm-thick, boron-doped ⟨100⟩ oriented silicon wafers. Prior to use, substrates were plasma cleaned for 5 min (March CS-1701) (100 mT of oxygen, and 20 W RF power). We coated substrates with hydroxy-terminated PS-*r*-PMMA random copolymer brush (M_w = 13 kg/mol, PS/PMMA 0.6:0.4, PDI = 1.5; 0.5% wt in toluene) *via* spin-casting (600 rpm, 45 s) in order to neutralize the surface and facilitate domain-ordering perpendicular to the wafer surface. Samples were baked in vacuum (<1 Torr, 200 °C) for at least 1 h and rinsed in toluene prior to coating with the block copolymer. Block copolymer thin films (Polymer Source, Inc.) were then applied by spin-casting the blended PS-*b*-PMMA solutions (all 1% wt in toluene) for 45 s at a rotation speed (between 1600−6000 rpm) selected to yield layers with a morphology extending uniformly through the entire film thickness. The film thicknesses studied in this work span a narrow range of thicknesses between ∼26 ± 2 nm (Figures 1 and 2). The block copolymer materials used in these experiments have the following characteristics. Cylindrical phase: M_w = 48 kg/mol, PS/PMMA 0.7:0.3, PDI = 1.1; M_w = 67 kg/mol, PS/PMMA 0.7:0.3, PDI = 1.1; M_w = 99 kg/mol, PS/PMMA 0.7:0.3, PDI = 1.1. Lamellar phase: M_w = 75 kg/mol, PS/PMMA 0.5:0.5, PDI = 1.1. We annealed block copolymer films in vacuum (<1 Torr, 200 °C) for 15 h. To improve contrast for SEM imaging, we cross-linked the PS block and removed the PMMA block from annealed copolymer films by exposure to ultraviolet light and rinsing in acetic acid (3 min) and deionized water (3 min). We imaged the samples by scanning electron microscopy (Hitachi S-4800), both top-down and at a 70° tilt angle.

Image Analysis. We computationally analyzed the self-assembled pattern morphology from SEM images using the Python programming language, and exploiting libraries for image manipulation (Python Image Library), numerical computations (numpy[39]), and plotting (matplotlib[40]).

To evaluate the relative fractional areal coverage of lamellar *versus* cylindrical morphologies for blended block copolymer thin films exhibiting both phases, we used image thresholding and particle-counting to isolate image structures, identifying lines (lamellae) and dots (cylinders) using a size cutoff. These characteristic structures were grown using a flood-fill method to segment the entire image into regions expressing the two morphologies. The resulting image was then overlaid atop the original to isolate one of the two morphologies for further analysis.

We determined the average domain spacing by applying a Fast Fourier Transform (FFT) to the image and fitting the fundamental peak position in the one-dimensional, circularly averaged spectrum. The average grain size for vertical lamellar morphologies (line patterns) was estimated using established methods.[41]

Conflict of Interest: The authors declare no competing financial interest.

Acknowledgment. The authors thank C. J. Hawker (U. C. Santa Barbara) for synthesis of the random copolymer used in these experiments. Research carried out at the Center for Functional Nanomaterials, Brookhaven National Laboratory, which is supported by the U.S. Department of Energy, Office of Basic Energy Sciences, under Contract No. DE-AC02-98CH10886.

Supporting Information Available: A schematic flow for SEM image analysis of fractional areal coverage and domain spacing determination, as well as the results of an experiment monitoring the time evolution fractional areal coverage of cylindrical phase in patterns formed from blended materials; details of the theoretical model of mixing in block copolymer blends used to understand the experimental results. This material is available free of charge *via* the Internet at http://pubs.acs.org.

REFERENCES AND NOTES

1. Black, C. T.; Ruiz, R.; Breyta, G.; Cheng, J. Y.; Colburn, M.; Guarini, K. W.; Kim, H.-C.; Zhang, Y. Polymer Self Assembly in Semiconductor Microelectronics. *IBM J. Res. Dev.* **2007**, *51*, 605–633.
2. Topham, P. D.; Parnell, A. J.; Hiorns, R. C. Block Copolymer Strategies for Solar Cell Technology. *J. Polym. Sci., Part B: Polym. Phys.* **2011**, *49*, 1131–1156.

3. Mecke, A.; Dittrich, C.; Meier, W. Biomimetic Membranes Designed from Amphiphilic Block Copolymers. *Soft Matter* **2006**, *2*, 751–759.
4. Checco, A.; Rahman, A.; Black, C. T. Robust Superhydrophobicity in Large Area Nanostructured Surfaces Defined by Block Copolymer Self Assembly. *Adv. Mater. (Weinheim, Ger.)* **2014**, *26*, 886–891.
5. Xu, T.; Kim, H.-C.; DeRouchey, J.; Seney, C.; Levesque, C.; Martin, P.; Stafford, C.; Russell, T. The Influence of Molecular Weight on Nanoporous Polymer Films. *Polymer* **2001**, *42*, 9091–9095.
6. Buck, E.; Fuhrmann, J. Surface-Induced Microphase Separation in Spin-Cast Ultrathin Diblock Copolymer Films on Silicon Substrate before and after Annealing. *Macromolecules* **2001**, *34*, 2172–2178.
7. Jeong, U.; Ryu, D. Y.; Kho, D. H.; Lee, D. H.; Kim, J. K.; Russell, T. P. Phase Behavior of Mixtures of Block Copolymer and Homopolymers in Thin Films and Bulk. *Macromolecules* **2003**, *36*, 3626–3634.
8. Kitano, H.; Akasaka, S.; Inoue, T.; Chen, F.; Takenaka, M.; Hasegawa, H.; Yoshida, H.; Nagano, H. Control of the Microdomain Orientation in Block Copolymer Thin Films with Homopolymers for Lithographic Application. *Langmuir* **2007**, *23*, 6404–6410.
9. Peng, J.; Gao, X.; Wei, Y.; Wang, H.; Li, B.; Han, Y. Controlling the Size of Nanostructures in Thin Films *via* Blending of Block Copolymers and Homopolymers. *J. Chem. Phys.* **2005**, *122*, 114706.
10. Hashimoto, T.; Koizumi, S.; Hasegawa, H. Ordered Structure in Blends of Block Copolymers. 2. Self-Assembly for Immiscible Lamella-Forming Copolymers. *Macromolecules* **1994**, *27*, 1562–1570.
11. Koizumi, S.; Hasegawa, H.; Hashimoto, T. Ordered Structure in Blends of Block Copolymers. 3. Self-Assembly in Blends of Sphere-or Cylinder-Forming Copolymers. *Macromolecules* **1994**, *27*, 4371–4381.
12. Abetz, V.; Goldacker, T. Formation of Superlattices *via* Blending of Block Copolymers. *Macromol. Rapid Commun.* **2000**, *21*, 16–34.
13. Spontak, R. J.; Fung, J. C.; Braunfeld, M. B.; Sedat, J. W.; Agard, D. A.; Kane, L.; Smith, S. D.; Satkowski, M. M.; Ashraf, A.; Hajduk, D. A. Phase Behavior of Ordered Diblock Copolymer Blends: Effect of Compositional Heterogeneity. *Macromolecules* **1996**, *29*, 4494–4507.
14. Zhao, J.; Majumdar, B.; Schulz, M. F.; Bates, F. S.; Almdal, K.; Mortensen, K.; Hajduk, D. A.; Gruner, S. M. Phase Behavior of Pure Diblocks and Binary Diblock Blends of Poly(ethylene)/Poly(ethylethylene). *Macromolecules* **1996**, *29*, 1204–1215.
15. Hadziioannou, G.; Skoulios, A. Structural Study of Mixtures of Styrene Isoprene Two- and Three-Block Copolymers. *Macromolecules* **1982**, *15*, 267–271.
16. Matsen, M. Immiscibility of Large and Small Symmetric Diblock Copolymers. *J. Chem. Phys.* **1995**, *103*, 3268–3271.
17. Matsen, M.; Bates, F. One-Component Approximation for Binary Diblock Copolymer Blends. *Macromolecules* **1995**, *28*, 7298–7300.
18. Kim, S. H.; Misner, M. J.; Russell, T. P. Solvent-Induced Ordering in Thin Film Diblock Copolymer/Homopolymer Mixtures. *Adv. Mater. (Weinheim, Ger.)* **2004**, *16*, 2119–2123.
19. Orso, K. A.; Green, P. F. Phase Behavior of Thin Film Blends of Block Copolymers and Homopolymers: Changes in Domain Dimensions. *Macromolecules* **1999**, *32*, 1087–1092.
20. Cheng, J. Y.; Ross, C. A.; Smith, H. I.; Thomas, E. L. Templated Self Assembly of Block Copolymers: Top Down Helps Bottom Up. *Adv. Mater. (Weinheim, Ger.)* **2006**, *18*, 2505–2521.
21. Koo, K.; Ahn, H.; Kim, S.-W.; Ryu, D. Y.; Russell, T. P. Directed Self-Assembly of Block Copolymers in the Extreme: Guiding Microdomains from the Small to the Large. *Soft Matter* **2013**, *9*, 9059–9071.
22. Hu, H.; Gopinadhan, M.; Osuji, C. O. Directed Self-Assembly of Block Copolymers: A Tutorial Review of Strategies for Enabling Nanotechnology with Soft Matter. *Soft Matter* **2014**, *10*, 3867–3889.
23. Bosworth, J. K.; Black, C. T.; Obert, C. K. Selective Area Control of Self-Assembled Pattern Architecture Using a Lithographically Patternable Block Copolymer. *ACS Nano* **2009**, *3*, 1761–1766.
24. Stoykovich, M. P.; Kang, H.; Daoulas, K. C.; Liu, G.; Liu, C.-C.; de Pablo, J. J.; Müller, M.; Nealey, P. F. Directed Self-Assembly of Block Copolymers for Nanolithography: Fabrication of Isolated Features and Essential Integrated Circuit Geometries. *ACS Nano* **2007**, *1*, 168–175.
25. Son, J. G.; Chang, J.-B.; Berggren, K. K.; Ross, C. A. Assembly of Sub-10-nm Block Copolymer Patterns with Mixed Morphology and Period Using Electron Irradiation and Solvent Annealing. *Nano Lett.* **2011**, *11*, 5079–5084.
26. Mansky, P.; Liu, Y.; Huang, E.; Russell, T.; Hawker, C. Controlling Polymer-Surface Interactions with Random Copolymer Brushes. *Science* **1997**, *275*, 1458–1460.
27. Han, E.; Stuen, K. O.; La, Y.-H.; Nealey, P. F.; Gopalan, P. Effect of Composition of Substrate-Modifying Random Copolymers on the Orientation of Symmetric and Asymmetric Diblock Copolymer Domains. *Macromolecules* **2008**, *41*, 9090–9097.
28. Hsu, H.-P.; Grassberger, P. Polymers Confined between Two Parallel Plane Walls. *J. Chem. Phys.* **2004**, *120*, 2034–2041.
29. Skvortsov, A.; Klushin, L.; Birshtein, T. Stretching and Compression of a Macromolecule under Different Modes of Mechanical Manupulations. *Polym. Sci., Ser. A* **2009**, *51*, 469–491.
30. Khokhlov, A.; Semenov, A. Liquid-Crystalline Ordering in the Solution of Long Persistent Chains. *Phys. A (Amsterdam, Neth.)* **1981**, *108*, 546–556.
31. Khokhlov, A.; Semenov, A. Liquid-Crystalline Ordering in the Solution of Partially Flexible Macromolecules. *Phys. A (Amsterdam, Neth.)* **1982**, *112*, 605–614.
32. Hsu, H.-P.; Binder, K. Semi-Flexible Polymer Chains in Quasi-One-Dimensional Confinement: A Monte Carlo Study on the Square Lattice. *Soft Matter* **2013**, *9*, 10512–10521.
33. Smyda, M. R.; Harvey, S. C. The Entropic Cost of Polymer Confinement. *J. Phys. Chem. B* **2012**, *116*, 10928–10934.
34. Silberberg, A. Distribution of Segments near the Surface of a Melt of Linear Flexible Macromolecules: Effect on Surface Tension. *J. Colloid Interface Sci.* **1988**, *125*, 14–22.
35. Silberberg, A. Distribution of Conformations and Chain Ends near the Surface of a Melt of Linear Flexible Macromolecules. *J. Colloid Interface Sci.* **1982**, *90*, 86–91.
36. Brown, H. R.; Russell, T. P. Entanglements at Polymer Surfaces and Interfaces. *Macromolecules* **1996**, *29*, 798–800.
37. DiMarzio, E. A. Proper Accounting of Conformations of a Polymer near a Surface. *J. Chem. Phys.* **2004**, *42*, 2101–2106.
38. Widin, J. M.; Schmitt, A. K.; Schmitt, A. L.; Im, K.; Mahanthappa, M. K. Unexpected Consequences of Block Polydispersity on the Self-Assembly of Aba Triblock Copolymers. *J. Am. Chem. Soc.* **2012**, *134*, 3834–3844.
39. Oliphant, T. E. Python for Scientific Computing. *Comput. Sci. Eng.* **2007**, *9*, 10–20.
40. Hunter, J. D. Matplotlib: A 2d Graphics Environment. *Comput. Sci. Eng.* **2007**, *9*, 0090–95.
41. Harrison, C.; Cheng, Z.; Sethuraman, S.; Huse, D. A.; Chaikin, P. M.; Vega, D. A.; Sebastian, J. M.; Register, R. A.; Adamson, D. H. Dynamics of Pattern Coarsening in a Two-Dimensional Smectic System. *Phys. Rev. E: Stat., Nonlinear, Soft Matter Phys.* **2002**, *66*, 011706.